Chemical Science

ROYAL SOCIETY OF CHEMISTRY

EDGE ARTICLE

View Article Online
View Journal | View Issue

Cite this: *Chem. Sci.*, 2025, **16**, 18318

All publication charges for this article have been paid for by the Royal Society of Chemistry

Exciton structure and dynamics in π-conjugated molecular wires

Naresh Duvva, Habtom B. Gobeze, Isaí Barboza-Ramos and Kirk S. Schanze *

Exciton and charge transport through π-conjugated oligomers and polymers is critical to the performance of organic electronic materials and essential for understanding carrier transport mechanisms on the nanoscale. This study applies photophysical methods to explore exciton structure and transport in π-conjugated molecules consisting of a diblock oligomer with terfluorene (**F3**) and tetrathiophene (**T4**) segments that are capped on either end with a boron dipyrromethene (**BDP**) unit. Two trichromophores were the focus of the investigation, **F3T4BDP** and **T4F3BDP**, where the sequence of the segments in the molecules is indicated by the acronyms. The molecules were probed by using steady-state and time-resolved absorption and fluorescence spectroscopy. Comparison of the absorption spectra of the trichromophores with model compounds (**F3**, **T4**, **BDP**) reveals that they exhibit absorption bands that can be assigned to transitions localized on the chromophore elements. Steady-state and time resolved fluorescence spectroscopy shows that excitation of the trichromophores leads to efficient transport of the excitation energy (exciton) to the **BDP** chromophore. By using femtosecond transient absorption (TA) spectroscopy it is shown that in **F3T4BDP** where the segments are arranged to allow vectorial exciton transfer (**F3** → **T4** → **BDP**) regardless of excitation wavelength exciton transfer to the **BDP** chromophore occurs in <1.5 ps. By contrast in **T4F3BDP** the energy landscape is more complex, and femtosecond TA results reveal that there is a bifurcation of the exciton between the **T4** and **BDP** units, and the partitioning ratio depends on the excitation wavelength.

Received 22nd May 2025
Accepted 26th August 2025

DOI: 10.1039/d5sc03704b

rsc.li/chemical-science

Introduction

π-Conjugated oligomers and polymers have been explored as "molecular wires" for efficient and long-range transport of electrons, holes and excitons.[1–8] Early studies explored the efficiency of electron or hole transfer *via* superexchange mediated tunneling, which revealed enhanced conductivity of π-conjugated bridges relative to fully saturated spacers.[9–15] More recent work examined charge transport through π-conjugated oligomers and polymers by single molecule conductivity.[4,16–25] These studies highlight that different π-conjugated electronic systems display semi-conductive to conductive behavior depending on their structure, and demonstrate the concept of molecular rectification.[2,16] Studies of excited state energy transfer reveal that π-conjugated electronic systems provide efficient pathways for singlet and, to a lesser extent, triplet exciton transport over long distances on fast timescales.[3,5,26–31] The importance of these fundamental processes to applications is evident in the widespread use of π-conjugated oligomers and polymers in a variety of optoelectronic devices including light emitting diodes,[32] solar cells,[33] photodetectors,[34] phototransistors[35] and sensors.[36]

Donor–bridge–acceptor (D–B–A) compounds represent a fundamental motif that has been used in the study of charge and energy transport within molecular systems.[9–11,37–46] In these architectures, a donor unit is electronically coupled to an acceptor through a π-conjugated or non-conjugated bridge, which mediates electronic communication between the termini.[6] These systems have been instrumental in exploring phenomena such as charge separation, recombination, and excitation energy transfer.[40,45] The bridge governs the mechanism and dynamics of transport, with π-conjugated bridges enabling coherent tunneling or hopping depending on their length and electronic structure.[6] Importantly, D–B–A frameworks have provided critical insights into vectorial electron and exciton transport, which underpin the function of molecular photodiodes,[23,47] and artificial photosynthetic assemblies.[46]

Our laboratory investigates charge and exciton delocalization and transport in π-conjugated oligomers and polymers.[29,30,48–50] These systems differ from previous work on D–B–A systems in the sense that the π-conjugated segments serve as both chromophore and bridge. In several recent studies, we explored the extent of excited state delocalization in "diblock oligomers",[51–53] which are π-conjugated molecules that

Department of Chemistry, University of Texas at San Antonio, San Antonio, TX 78249, USA. E-mail: kirk.schanze@utsa.edu

feature two defined segments with distinct frontier π-orbital energies and HOMO–LUMO gaps. This work provided evidence that excitation wavelength photoselection can be used to control the initial localization of an exciton, even in fully π-conjugated systems.[52] We established that wavelength photoselection could be used to control whether electron or energy transfer occurs in the same π-conjugated system.[54,55]

The current study examines a set of π-conjugated diblock oligomers which feature a terfluorene segment linked to a tetrathiophene segment (**F3T4**). The **F3** and **T4** segments have different frontier orbital energy levels and bandgaps, and thus it is possible to selectively excite the **F3** or **T4** π-conjugated segment. Two regioisomeric diblock oligomers are end functionalized with a boron dipyrromethene (**BDP**) chromophore which acts as a fluorescent energy acceptor that is attached to either end of the diblock oligomer. The objective of this work is to apply steady-state and femtosecond transient absorption (**TA**) spectroscopy to investigate the spatial extent, localization and dynamics of excitation energy through the fully π-conjugated molecules following excitation at wavelengths corresponding to the **F3** and **T4** segments. The results of the study provide clear evidence for exciton localization on the wide gap **F3** segment at early times (<1 ps) following photoexcitation. In the oligomer where the **F3**, **T4** and **BDP** units are aligned for vectorial energy transfer, the π-conjugated oligomer acts as a molecular wire, funneling the excitation energy to the **BDP** chromophore on an ultrafast timescale. However, in the regioisomer where the **BDP** is attached to the opposite end of the diblock segment, directional energy flow is interrupted and the results show that the transport is bifurcated, resulting in a partitioning of the energy between the two ends of the oligomer. The results provide unique insights into the electronic structure and dynamics of exciton localization and transport in fully π-conjugated electronic systems that are structurally related to conjugated polymers that are widely used in optoelectronic applications.

Results

Design and synthesis

This study explored the series of fully π-conjugated molecules shown in Chart 1. These molecules feature the three chromophoric units, terfluorene (**F3**), tetrathiophene (**T4**) and boron dipyrromethene (**BDP**). The two key molecules of interest feature all three of the units (**F3T4BDP** and **T4F3BDP**) with different connectivity (regioisomers), along with three model chromophores that contain two of the three units (**F3T4**, **F3BDP** and **T4BDP**).

The objective of this study was to apply steady-state and ultrafast time-resolved spectroscopy to study exciton structure, delocalization and energy transport dynamics in fully π-conjugated chromophore systems. Towards that end, we designed the diblock oligomer **F3T4** which features *tert*-fluorene (**F3**) and *tetra*-thiophene (**T4**) segments (chromophores) that are linked to enable full π-conjugation between the segments. As will be delineated in more detail below, these two segments have distinct HOMO–LUMO gaps, with **F3** absorbing in the near-UV region and **T4** in the blue region of the visible. Then we utilized the boron dipyrromethene (**BDP**) as a third chromophore element, attached to either end of the **F3T4** unit. **BDP** has a lower HOMO–LUMO gap compared to either **F3** or **T4**, and a distinct emission spectrum and high fluorescence quantum yield; therefore, it acts as an energy acceptor and "signaling chromophore". The goal was to understand the dynamics of exciton localization and transport through the fully conjugated molecule and how it depends on the structure, *e.g.* whether the **BDP** signaling chromophore is attached to the **T4** terminus or the **F3** terminus, *e.g.* Scheme 1.

All molecules were synthesized by using sequential Pd-catalyzed coupling reactions, first building the suitably end-functionalized **F3**, **T4** and **BDP** units and then linking them using another round of Pd-coupling reactions. Complete details, including synthetic schemes, descriptions and spectroscopic characterization data are provided in the SI.

Absorption and fluorescence properties

Absorption spectra were obtained for the full suite of molecules shown in Chart 1 in toluene solution. The set of normalized absorption spectra are shown in Fig. 1, and the spectra plotted on a molar absorptivity scale (ε, $M^{-1}cm^{-1}$) are shown in Fig. S46. First, Fig. 1a displays absorption spectra of the individual chromophores with well-defined bands for **F3** at λ_{max} ~350 nm, **T4** with λ_{max} ~378 nm and **BDP** with λ_{max} ~502 nm. Second, Fig. 1b compares spectra of diblock oligomer **F3T4** and the bichromophores **F3BDP** and **T4BDP** which contain the individual π-conjugated oligomers linked to **BDP**.

In the diblock oligomer **F3T4** two absorption maxima are distinguished at λ_{max} ~366 nm and 421 nm. These bands correspond approximately to transitions arising from the **F3** and **T4** segments, respectively. However, it is evident that both band maxima are red-shifted compared to the individual units (Fig. 1a) which is attributed to the interactions (delocalization) between the **F3** and **T4** conjugated segments. This notion is supported by time-dependent density functional theory (TD-DFT) calculations (see SI, Fig. S58, Tables S3 and S4) which reveal that the absorption bands correspond to transitions between frontier orbitals that are localized primarily on the respective π-conjugated segments, but with some delocalization/interaction between them. Taken together, the experimental and computational data reveal that excitation of **F3T4** into the short wavelength absorption (~360 nm) gives rise to an excited state that is predominantly localized on the **F3** segment, but has a degree of delocalization into the **T4** segment. By contrast, excitation of **F3T4** into the longer wavelength absorption feature (~420 nm) directly accesses the lowest excited state of the chromophore, which is mainly localized on the **T4** segment, but has some delocalization in to the **F3** segment.

The bichromophoric molecules **F3BDP** and **T4BDP** display absorption bands associated with the π-conjugated **F3** or **T4** segments, along with a narrow absorption band with peak at 505 nm due to **BDP** (Fig. 1b). Fig. 1c compares the normalized absorption spectra of the trichromophores **F3T4BDP** and **T4F3BDP**. The spectra of these molecules are generally similar,

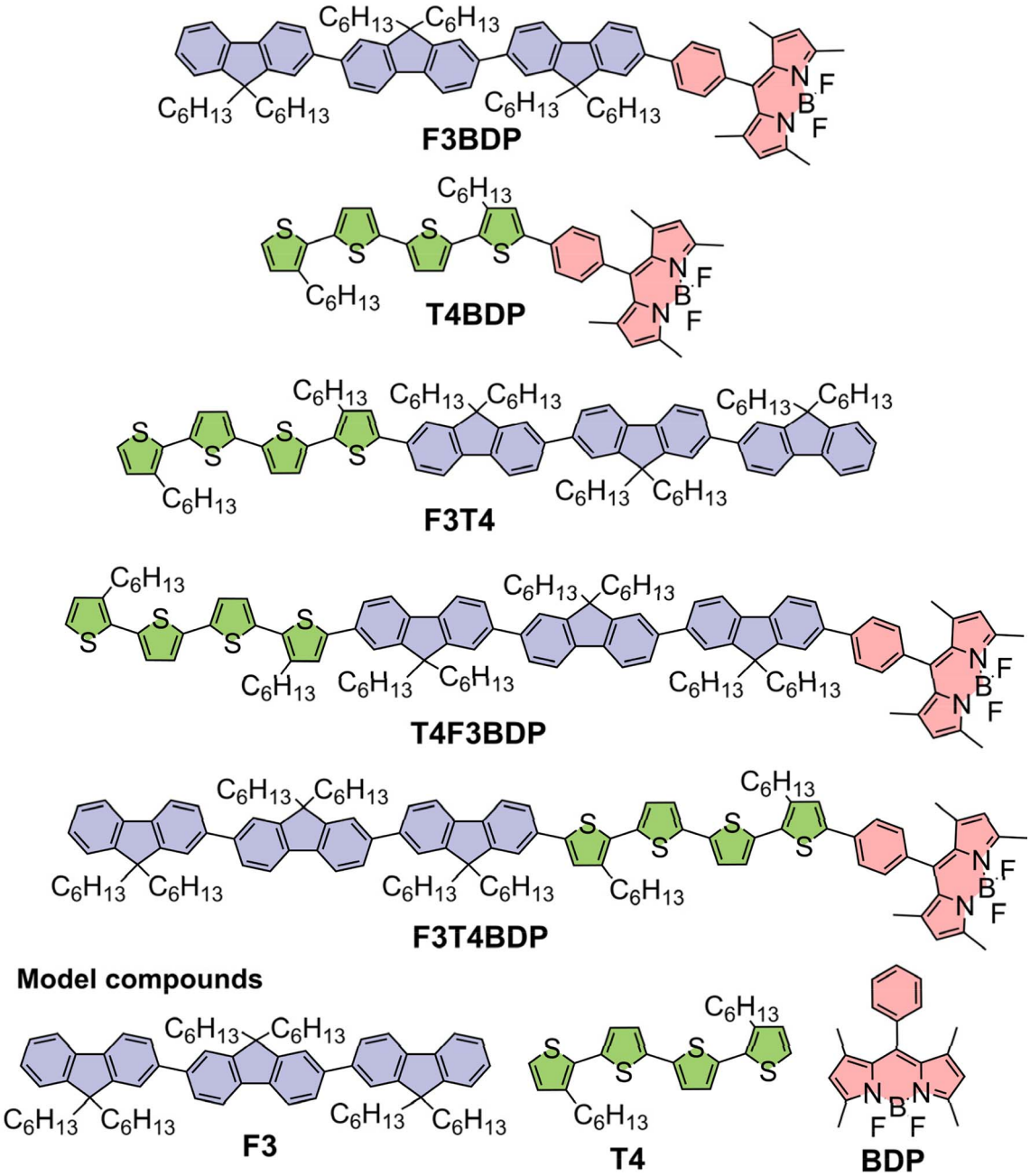

Chart 1 Chemical structures of the oligomers studied.

with broad absorption features that can be ascribed to **F3** at λ ~355–375 nm range, **T4** at λ ~420–425 nm and **BDP** at λ ~505 nm. It is notable that the absorption attributed to the **T4** segment is red shifted in **F3T4BDP**, suggesting that in this configuration the **T4** localized transitions are at a slightly lower energy compared to **T4F3BDP**.

The fluorescence emission of the monomers, di- and tri-chromophores were measured in toluene solution, and the spectra are collected in Fig. 2. The fluorescence spectra were collected at different excitation wavelengths (355 nm, 400 nm, and 490 nm), allowing excitation of the various subunits of the di- and tri-chromophores. Table 1 contains a summary of the photophysical properties of the compounds, including fluorescence quantum yields (Φ_{fl}) and lifetimes (τ_{fl}). Fig. 2a compares the spectra of **F3**, **F3T4** and **F3BDP** with excitation at 355 nm, which corresponds to the absorption of the **F3** unit. Note that **F3** displays an emission with a peak at 395 nm that is associated with the $^1\pi,\pi^*$ state of the **F3** chromophore. The diblock oligomer **F3T4** displays a weak, broad emission at ~420 nm corresponding to **F3**, and a stronger, structured emission with two maxima at 521 and 552 nm that is believed to arise from the **T4** segment in **F3T4**. The emission of **F3BDP** is a single narrow band with λ_{max} = 517 nm, that corresponds to emission from the **BDP** unit (compare with Fig. 2c). The latter result

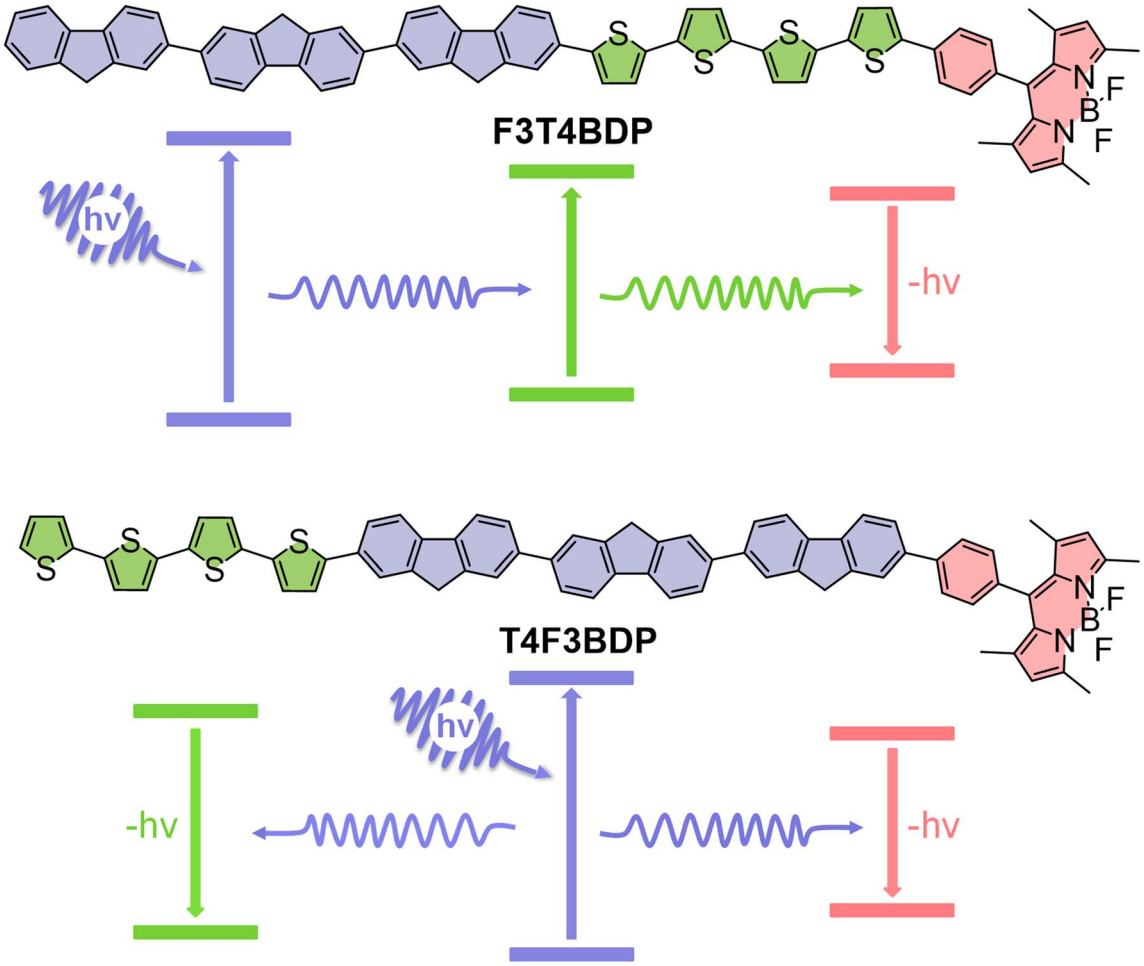

Scheme 1 Diagram of exciton transport in the oligomers.

demonstrates that **F3** to **BDP** energy transfer is highly efficient in **F3BDP** (*vide infra*).

Fig. 2b compares the fluorescence of **T4**, **F3T4** and **T4BDP** with excitation at 400 nm, which corresponds to the **T4** unit's absorption. This comparison reveals several important features. First, it is evident that the fluorescence of **F3T4** is red shifted ~60 nm compared to that of **T4**. This clearly indicates that the energy of the lowest excited state in **F3T4** is lower compared to **T4**, suggesting that even though the $^1\pi,\pi^*$ excitation is mainly localized in the **T4** unit in **F3T4**, the excited state is stabilized by delocalization into **F3**. Second, the emission of **T4BDP** is similar to that of **BDP** and **F3BDP**, which reveals that **T4** to **BDP** energy transfer is highly efficient (*vide infra*).[56]

Fig. 2d–f compare the fluorescence of the tri-chromophores **F3T4BDP** and **T4F3BDP** with excitation wavelengths of 355 nm, 400 nm and 490 nm, corresponding to the **F3**, **T4** and **BDP** units, respectively. Notably, in each case the fluorescence is dominated by the **BDP** chromophore with λ_{max} ~515 nm, regardless of excitation wavelength. This finding suggests that in the trichromophores, energy transfer occurs efficiently to the lowest energy state localized on the **BDP** chromophore (*vide infra*). However, there is a noteworthy feature that is present in the fluorescence of **F3T4BDP**, namely a broad, tailing emission extending from the peak of the **BDP** feature to 700 nm. This feature is believed to arise from the **T4** localized emission in the **F3T4** unit that is linked to **BDP**. Interestingly, this feature is not apparent in **T4F3BDP**, which suggests that it requires the **T4** and **BDP** chromophores to be adjacent. This point will be discussed further below.

Further insights into the photophysics of the polychromophores comes from analysis of the fluorescence quantum yield and lifetime data in Table 1. First, it is seen that the lifetime of **F3T4** is intermediate between the lifetimes of **F3** and **T4**. Second, for all polychromophores that contain a **BDP** unit, the fluorescence lifetimes are substantially longer, ranging from 1.75 ns (**T4F3BDP**) to 3.28 ns (**BDP**). This is consistent with the fluorescence emanating from a singlet excited state that is localized on the **BDP** chromophore (Table 1). However, it is noteworthy that in every case of the polychromophores that contain the **BDP** unit the lifetimes and quantum yields are lower compared to the reference chromophore (**BDP**, τ = 3.28 ns). This observation suggests that there are additional non-radiative decay channels active in the polychromophores that reduce the lifetime of the **BDP** localized excited state. As discussed in more detail below, this is believed to be due in part to quenching by photoinduced charge transfer from the π-conjugated units to **BDP**.

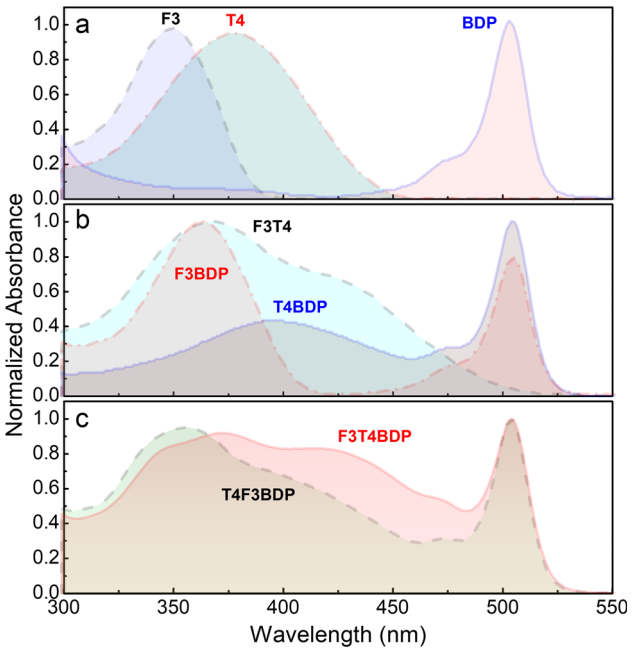

Fig. 1 Normalized absorption spectra in toluene solution. (a) **F3**, **T4** and **BDP**. (b) **F3BDP**, **F3T4** and **T4BDP**. (c) **F3T4BDP** and **T4F3BDP**.

Excitation spectra were collected for the trichromophores **F3T4BDP** and **T4F3BDP** monitoring the emission from the **BDP** chromophore at 517 nm. The excitation spectra are compared to the normalized absorption spectra in Fig. 3. Here it can be seen that the shapes of the excitation spectra generally mirror the absorption for both molecules; this result indicates regardless of the excitation wavelength energy transfer to the **BDP** signalling chromophore is efficient. Nevertheless, it is noteworthy that for both **F3T4BDP** and **T4F3BDP** the excitation spectrum amplitude is lower than the absorption by 15–20% at wavelengths <475 nm. This reveals an inefficiency in the **BDP** fluorescence when excitation is at shorter wavelengths; as discussed below it is believed that this may be due to photoinduced electron transfer (ET) pathways that competes with energy transfer.

Electrochemistry

As noted above, photoinduced ET may be involved in the photophysics of the polychromophores. As such we carried out electrochemical analysis of the molecules to understand their redox properties. This information is used below to calculate the relative energetics of various charge transfer excited states. The electrochemical studies were carried out using cyclic voltammetry (CV) in dichloromethane solution at a glassy carbon electrode, and the potentials are listed *vs.* ferrocene/ferrocenium (Fc/Fc^+, internal standard). Fig. S49 shows the cyclic voltammograms of the molecules and Table S1 summarizes the electrochemical potentials data along with the estimated HOMO and LUMO energy levels. The electrochemical data show that model compounds **F3**, **T4**, and **BDP** have first oxidation potentials at 0.78, 0.52, and 0.74 V, respectively and the reduction of **BDP** was at −1.71 V (potentials *vs.* Fc/Fc^+ reference, Fc = ferrocene). Under similar experimental

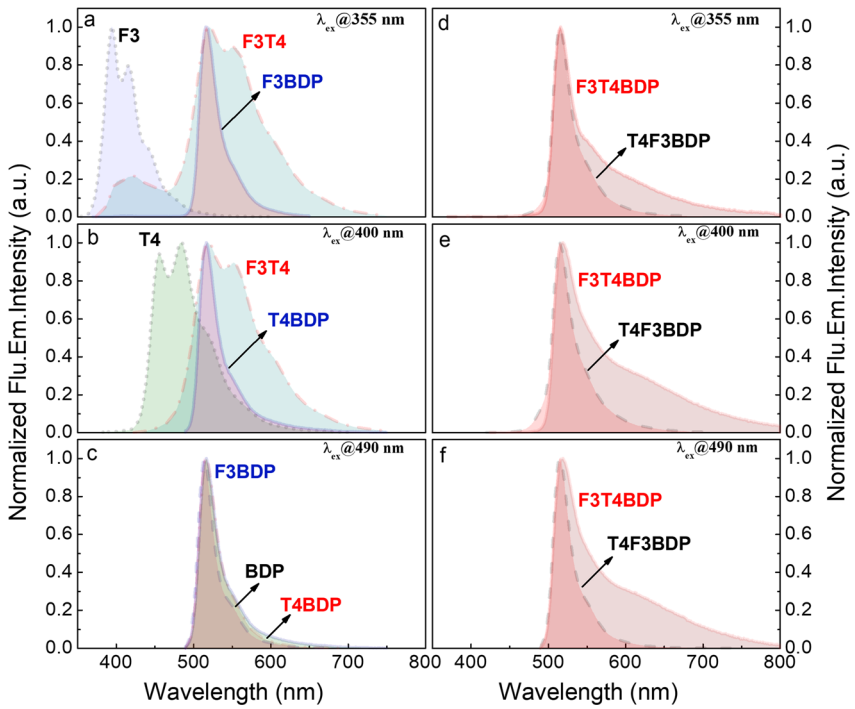

Fig. 2 Normalized fluorescence spectra of oligomers in toluene solution. (a) **F3**, **F3T4** and **F3BDP**, λ_{ex} = 355 nm. (b) **T4**, **F3T4** and **T4BDP**, λ_{ex} = 400 nm. (c) **F3BDP**, **T4BDP** and **BDP**, λ_{ex} = 490 nm. (d) **F3T4BDP** and **T4F3BDP**, λ_{ex} = 355 nm. (e) **F3T4BDP** and **T4F3BDP**, λ_{ex} = 400 nm. (f) **F3T4BDP** and **T4F3BDP**, λ_{ex} = 490 nm.

Table 1 Photophysical properties of oligomers[a]

Compound	Abs λ_{max}/nm	$\varepsilon^{b}/10^4$ mol^{-1}cm^{-1}	FL λ_{max}/nm	Φ_{fl}	τ^{d} ns
F3	350	13.5	395, 416	0.96	0.64[e]
T4	378	2.69	456, 485	0.31	0.32[f]
BDP	502	16.6	514	0.56[c]	3.28[g]
F3T4	366, 421	7.9 (366), 5.4 (421)	423, 521, 552	0.54	0.52[e]
F3BDP	364, 505	13.3 (364), 10.5 (505)	517	0.39[c]	2.81[e]
T4BDP	395, 505	6.2 (395), 14.4 (505)	517	0.36[c]	2.01[f]
F3T4BDP	374, 420, 504	11.5 (374), 10.5 (420), 12.6 (504)	517	0.25[c]	1.8[e]
T4F3BDP	354, 420, 504	11.8 (354), 6.9 (420),12.4 (504)	515	0.33[c]	2.8[e]

[a] Measured in toluene solution. [b] Values in parenthesis are the wavelengths (nm) at which the molar extinction coefficient is reported. [c] Reported quantum yields are for **BDP** fluorescence at 490 nm. [d] Lifetimes are essentially independent of excitation wavelength, see Fig. S51–S53 for full decays and analysis. [e] Excitation at 350 nm. [f] Excitation at 400 nm. [g] Excitation at 490 nm.

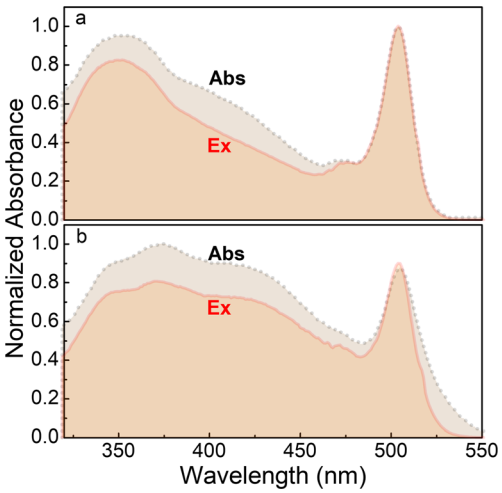

Fig. 3 Overlay of excitation (solid, red – Ex) and absorption (dash dot, black – Abs) spectra of (a) **T4F3BDP** and (b) **F3T4BDP** in toluene (λ_{em} = 517 nm). The excitation spectra were corrected for the instrument response function and were normalized with respect to the absorption spectra at 517 nm.

conditions, the bichromophores exhibit first oxidation potentials at 0.37 V (**F3T4**), 0.74 V (**F3BDP**), and 0.43 V (**T4BDP**), and the trichromophores **T4F3BDP** at 0.51 V and **F3T4BDP** at 0.52 V. In all cases of compounds that contain the **T4** unit, the first oxidation potential is within ~75 mV of 0.45 V, and as such it is associated with that conjugated segment.

Ultrafast transient absorption spectroscopy. 1. bichromophores

To explore the structure and dynamics of the excited states produced by excitation of the polychromophores, we applied femtosecond transient absorption (TA) spectroscopy with probe in the near-UV, visible and near-infrared (NIR) regions. These studies were carried out with the conjugated oligomers dissolved in toluene solution using excitation wavelengths tuned to selectively excite the different π-conjugated chromophores. In the main text below, we focus on the time-evolving TA spectra and kinetics at specific wavelengths, as we believe this approach provides greater clarity for the reader.

First, we focus on the TA data for the **T4BDP** bichromophore excited at 420 nm shown in Fig. 4. For this compound, excitation at 420 nm selectively excites the **T4** unit (see absorption spectrum in Fig. 1b). As seen in Fig. 4a, at ~1 ps after excitation the TA spectrum is dominated by a narrow, negative absorption at 505 nm and a positive excited state absorption (ESA) in the red/near-IR, with a peak at ~750 nm and a shoulder at ~1000 nm. The 750 nm ESA is due to the singlet excited state of the **T4** segment (^{1}**T4***, see Fig. S54), and the negative feature at 505 is due to the ground state bleach (GSB) of the **BDP** chromophore. Within a few ps, the 750 nm ESA due to the ^{1}**T4*** decays, and it is replaced by a broader and weaker, red-shifted near-IR band at 1000 nm, accompanied by the GSB of the **BDP** chromophore. Fig. 4b shows the TA kinetics monitored at 841 nm in the near-IR near the ESA peak associated with the excited state ^{1}**T4***. This shows that there is an ultrafast decay with τ ~300 fs followed by a slower relaxation with bi-exponential kinetics (316 ps and 1.6 ns). These data can be explained by the following processes (refer to eqn (1) and (2) below). First, 420 nm excitation generates the singlet excited state that is mainly localized on the **T4** segment, eqn (1). Then this state decays *via* two competing pathways:

$$\mathbf{T4BDP} + h\nu(420\ \text{nm}) \rightarrow (^1\mathbf{T4^*})\mathbf{BDP} \quad (1)$$

$$(^1\mathbf{T4^*})\mathbf{BDP} \rightarrow \mathbf{T4}(^1\mathbf{BDP^*}) \rightarrow \mathbf{T4BDP} + h\nu + \Delta \quad (2a)$$

$$(^1\mathbf{T4^*})\mathbf{BDP} \rightarrow (\mathbf{T4}^+)(\mathbf{BDP}^-) \rightarrow \mathbf{T4BDP} + \Delta \quad (2b)$$

One pathway involves energy transfer to the BDP chromophore (2a),[56] and the other involves photoinduced electron transfer to produce a charge separated state (2b). Evidence for pathway 2b comes from the appearance of the NIR absorption feature at 1000 nm that is prominent at 10 ps delay and longer which can be assigned to the **T4**-cation radical ($\mathbf{T4}^+$).[54] This charge separated state is likely the origin of the intermediate decay time that comes from the kinetic fit in Fig. 4b (316 ps). The driving force for the photoinduced charge transfer process in eqn (2b) can be estimated from the electrochemical and photophysical data in Tables 1 and S1 and is −0.50 eV.

Transient absorption of the **F3BDP** bichromophore (Fig. S57) with excitation at 363 nm corresponding to the **F3** segment

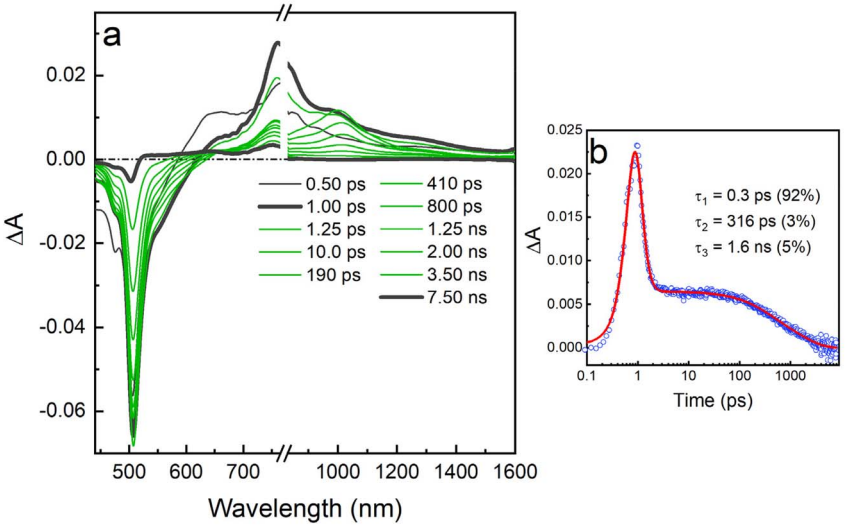

Fig. 4 Femtosecond TA difference spectra of T4BDP in toluene solution with excitation at 420 nm. (a) Visible-near-infrared spectra as a function of delay time ranging from 500 fs to 7.5 ns. (b) TA kinetics at 841 nm, symbols show the experimental data and solid line is fit with parameters shown in inset. Evolution associated difference spectra (EADS) obtained from global analysis of data is provided in Fig. S59 in SI.

absorption reveals that there is ultrafast excitation transfer (~500 fs) to produce the **BDP** localized singlet excited state, eqn (3).

$$\mathbf{F3BDP} + h\nu(363\text{ nm}) \rightarrow (^1\mathbf{F3}^*)\mathbf{BDP} \rightarrow \mathbf{F3}(^1\mathbf{BDP}^*) \quad (3)$$

Taken together, the results on the two bichromophores that contain either **T4** or **F3** linked to the **BDP** chromophore reveal that the predominant pathway is energy transfer with a time constant ≤ 500 fs to produce the **BDP** localized singlet excited state. This finding is in accord with a previous study of a bichromophore featuring **T4** linked to **BDP** underwent **T4** to **BDP** energy transfer with τ ~120 fs ($k \sim 8 \times 10^{12}$ s^{-1}).[56]

The diblock oligomer **F3T4** features two distinct π-conjugated segments, one based on the terfluorene (**F3**) unit and the second based on the tetrathiophene (**T4**) unit. As noted above, the HOMO–LUMO gaps of the **F3** and **T4** segments are distinct, with **F3** displaying absorption at 350 nm, and **T4** at 378 nm (Fig. 1a). The ground state absorption spectrum of the diblock oligomer **F3T4** (Fig. 1b) displays absorption features that can be attributed to the **F3** and **T4** segments. Although the two π-conjugated segments are π-conjugated *via* a C–C bond, we hypothesized that at very early times following near-UV excitation, it may be possible to distinguish an excited state that is predominantly localized on the **F3** segment following excitation into the **F3** absorption in the near-UV region.

The time-resolved TA spectra for **F3T4** following 363 nm excitation (corresponding to the **F3**-localized absorption feature, Fig. 1b) are shown in Fig. 5a. The spectra are dominated by negative absorption at 420 nm corresponding to the GSB of the **T4** absorption feature, a second negative feature ranging from 500–575 nm corresponding to stimulated emission (SE), and a strong, broad absorption in the near-IR with a peak at 910 nm. All these features can be associated with a $^1\pi,\pi^*$ excitation that is mainly on the **T4** segment, but with some delocalization into the **F3** unit. Note that the 420 nm GSB feature corresponds to the long wavelength absorption attributed to **T4**, and the near-IR absorption is similar, but red-shifted, from that observed for the **T4** model compound (Fig. S54). To probe the dynamics of the excited state following excitation, we plotted the TA kinetics at 919 nm in Fig. 5b. This plot compares the evolution of the TA at 919 nm for samples with excitation at 363 nm (F3 absorption) and 420 nm (**T4** absorption) (the full set of TA spectra for 420 nm excitation is in Fig. S56). Fig. 5b shows that the near-IR absorption grows rapidly with both excitation wavelengths. The kinetic fits suggest a slightly faster risetime (500 fs) for excitation at 420 nm corresponding to the **T4** segment absorption, compared with the risetime (900 fs) for excitation into the **F3** absorption band at 363 nm. While the difference in rise times is small, the slower rise of the near-IR band with 363 nm excitation is consistent with the notion that there may be some initial localization of the exciton on the **F3** segment.

Ultrafast transient absorption spectroscopy. 2. trichromophores

Transient absorption was applied to the two trichromophores, **F3T4BDP** and **T4F3BDP**, with the aim to investigate the relationship between the oligomer structure and excitation wavelength on the exciton localization, transport and dynamics. Note that the key difference in the two oligomers is the location of the **BDP** chromophore with respect to the **F3T4** diblock oligomer. In **F3T4BDP**, the **BDP** unit is attached to the **T4** "end", whereas in **T4F3BDP**, the **BDP** is attached to the **F3** "end". As shown below, the orientation has a substantial effect on the exciton dynamics and transport within the trichromophores.

Fig. 6 provides a summary of the transient absorption spectra and dynamics of **F3T4BDP** with excitation at 350 nm (Fig. 6a–c) and 420 nm (Fig. 6d–f). Qualitatively, the spectra and

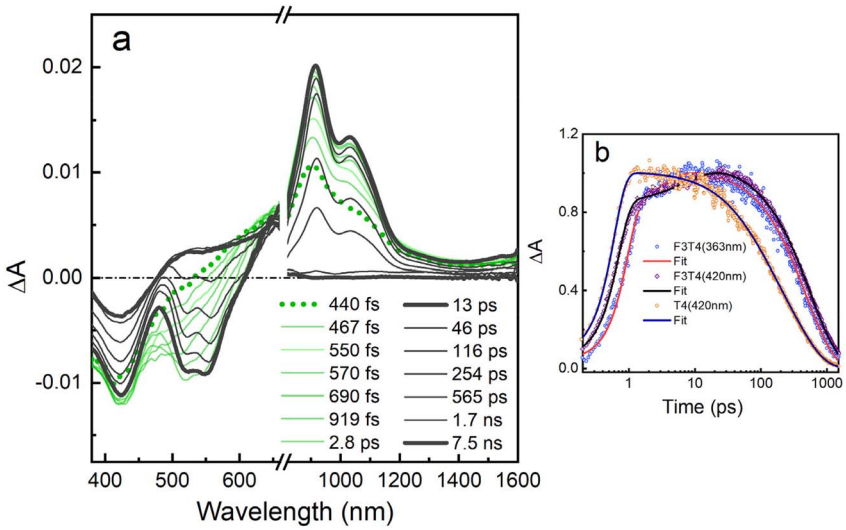

Fig. 5 (a) Femtosecond TA spectra of **F3T4** in toluene solvent with excitation at 363 nm. Delay times range from 440 fs to 7.5 ns, see legend inset for time labels. (b) TA kinetics at 919 nm for **T4** (λ_{ex} = 420 nm), **F3T4** (λ_{ex} = 363 nm) and **F3T4** (λ_{ex} = 420 nm). Evolution associated difference spectra (EADS) obtained from global analysis of data is provided in Fig. S60 in SI.

dynamics are similar for the two different excitation wavelengths, suggesting that photoselection within the **T4F3** diblock oligomer does not have a significant effect. For each excitation wavelength, the spectra feature two negative absorptions in the visible, namely at 425 nm corresponding to **F3T4** GSB and 507 nm due to **BDP** GSB. The early time spectra also feature the prominent near-IR absorption bands (905 and 1020 nm) associated with the **F3T4** excited state that is mainly localized on the **T4** segment. The dynamics of the visible GSB attributed to **BDP** (507 nm) and the near-IR absorption attributed to the **F3T4** excited state (905 nm) are shown in panels on the right-hand side of Fig. 6 and are revealing as to the excited state dynamics. First, it is evident that the 507 nm GSB feature rises within 400–500 fs regardless of excitation wavelength. This

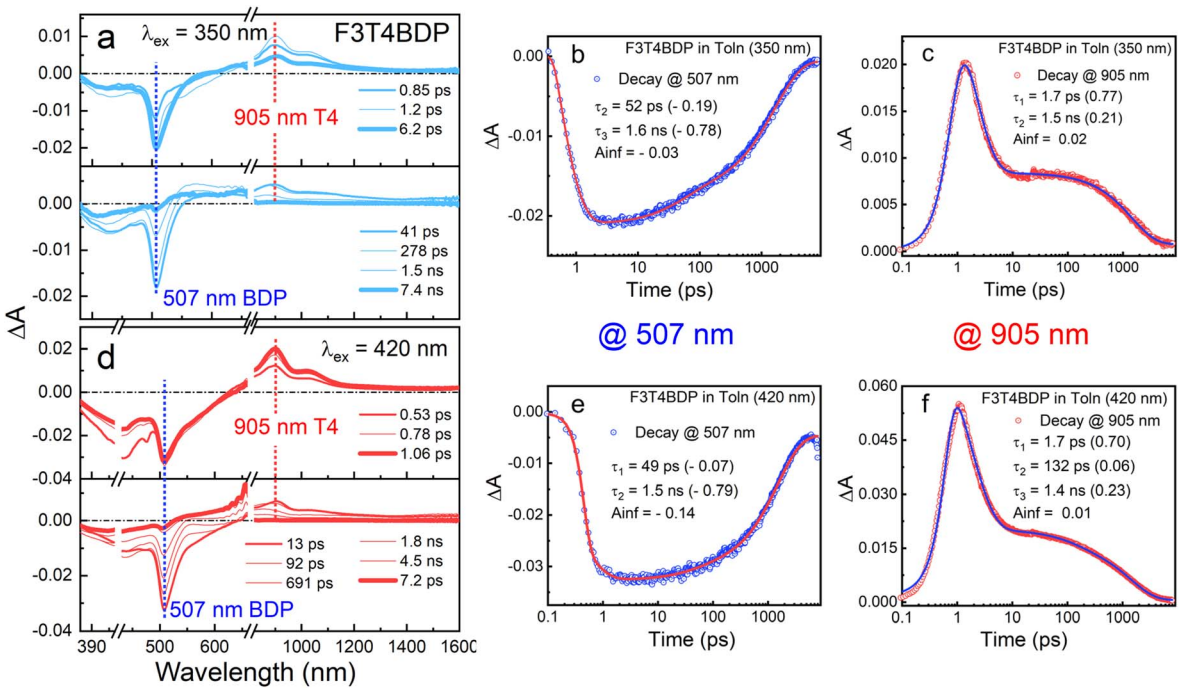

Fig. 6 Femtosecond TA spectra of **F3T4BDP** in toluene solution. (a) λ_{ex} = 350 nm. (d) λ_{ex} = 420 nm. Note that in (a) and (d) upper panels show early delay times and lower panels show longer delay times. (b) TA kinetics at 507 nm, λ_{ex} = 350 nm. (c) TA kinetics at 905 nm, λ_{ex} = 350 nm. (e) TA kinetics at 507 nm, λ_{ex} = 420 nm. (f) TA kinetics at 905 nm, λ_{ex} = 420 nm. Evolution associated difference spectra (EADS) obtained from global analysis of visible region data is provided in Fig. S61 in SI.

suggests that energy transfer from the **F3T4** segment to the **BDP** chromophore is ultrafast, and is not strongly dependent on the excitation wavelength. The GSB feature at 507 nm due to **BDP** decays on the nanosecond timescale with a lifetime of approximately 1.5–1.6 ns, closely matching the fluorescence lifetime of **F3T4BDP** (Table 1, τ ~1.7 ns). Next, the near-IR absorption feature that is due to the **F3T4** chromophore displays an ultrafast decay (τ ~1.7 ps) followed by a much slower decay lifetime τ ~1.5 ns that is like that for the **BDP** GSB. Taken together, these results suggest that for **F3T4BDP** excitation of the **F3T4** oligomer segment is followed by ultrafast transfer of the excitation to the **BDP** chromophore. The existence of the short-lived, prominent near-IR absorption suggests that some energy remains localized in the **T4** segment, but that it funnels into the BDP unit on the 1.7 ps timescale ($k \sim 6 \times 10^{11}$ s^{-1}). Also of note is the fact that the slow decay component in the near-IR absorption suggests that some excitation energy remains on the **F3T4** unit on a timescale similar to the lifetime of the **BDP** chromophore. As noted below, we believe that this feature arises due to the establishment of an excited state equilibrium, which is established between ^{1}**BDP*** and ^{1}(**F3T4**)*.

The femtosecond TA spectra for **T4F3BDP** in which the **BDP** chromophore is linked to the **F3** end of the **F3T4** oligomer is substantially different compared to that for the regioisomer **F3T4BDP**. Specifically, as shown in Fig. 7, the TA spectra of **T4F3BDP** are distinct and they reveal a subtle excitation wavelength dependence that indicates that there is some photoselection that occurs depending on which segment within the **F3T4** oligomer is initially photoexcited. First, inspection of Fig. 7a–c shows that when the oligomer is excited at 350 nm, the TA spectra reveal two negative absorptions in the visible, namely at ~400 nm corresponding to **F3T4** GSB and 507 nm due to **BDP** GSB. Importantly, the negative absorption that peaks at 507 nm is broader on the long wavelength side compared to its appearance in **F3T4BDP** (*cf.* Fig. 6a). This broadening is due to the strong stimulated emission (SE) arising from the **F3T4** segment. The spectra also exhibit the prominent near-IR band at 905 nm which is associated with excitation of the **F3T4** oligomer. Remarkably, this near-IR absorption feature for **T4F3BDP** lives much longer than in **F3T4BDP**; as seen in Fig. 7c, the absorption at 905 nm exhibits a decay lifetime of 245 ps. This result clearly shows that some fraction of the excitation remains on the **F3T4** oligomer at long times following excitation. Nevertheless, some fraction of the excitation energy arrives at the **BDP** chromophore, as illustrated by the GSB at 507 nm, which decays with the relatively longer lifetime of 2.8 ns in agreement with the fluorescence lifetime (Table 1).

When **T4F3BDP** is excited at 420 nm, corresponding to the **T4** absorption band, several differences emerge compared to 350 nm excitation (compare Fig. 7a and c). Most notably, the negative absorption feature attributed to ground-state bleach (GSB) of the **BDP** chromophore and stimulated emission (SE) from the **F3T4** oligomer is even broader and red-shifted (~530 nm). This indicates that the dominant contribution to the negative signal now comes from **F3T4** SE rather than **BDP** GSB. The positive TA band in the near-IR, associated with **F3T4**,

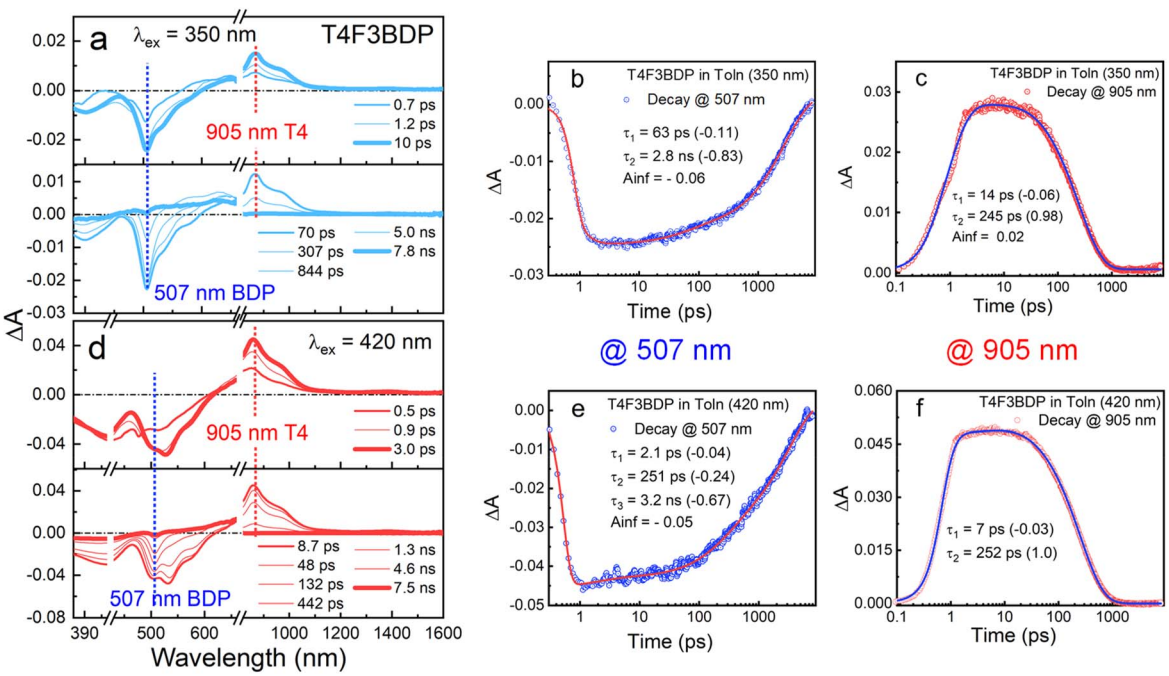

Fig. 7 Femtosecond TA spectra of **T4F3BDP** in toluene solution. (a) λ_{ex} = 350 nm. (d) λ_{ex} = 420 nm. Note that in (a) and (d) upper panels show early delay times and lower panels show longer delay times. (b) TA kinetics at 507 nm, λ_{ex} = 350 nm. (c) TA kinetics at 905 nm, λ_{ex} = 350 nm. (e) TA kinetics at 507 nm, λ_{ex} = 420 nm. (f) TA kinetics at 905 nm, λ_{ex} = 420 nm. Evolution associated difference spectra (EADS) obtained from global analysis of visible region data is provided in Fig. S62 in SI.

decays with a 252 ps lifetime, similar to that observed under 350 nm excitation. However, at 507 nm, the visible-region decay is more complex under 420 nm excitation, exhibiting tri-exponential kinetics with two longer components of 251 ps and 3.2 ns. The 251 ps component matches the near-IR decay lifetime, supporting the interpretation that part of the visible-region negative signal arises from **F3T4** SE.

The effect of wavelength photoselection on the TA spectra is more apparent by inspection of the EADS from global analysis (Fig. S62). Here it is seen that the GSB due to the **BDP** chromophore (3.2 ns component) is more pronounced (larger amplitude) with 350 nm compared to 420 nm excitation. Additionally, the broad negative component associated with SE from **F3T4** (240 ps component) is by far the dominant component with 420 nm excitation.

Taken together, the femtosecond TA studies of the two trichromophores reveal divergent photophysical behavior. In **F3T4BDP**, the orientation of the chromophores provides for a vectorial transfer of the excitation energy (*e.g.* Scheme 1) and the TA spectra and dynamics support the notion that excitation leads to very rapid and efficient transfer of the excitation to the **BDP** chromophore. By contrast, in **T4F3BDP**, the spectroscopy and dynamics are more complex, and they suggest that there is a partitioning of the energy between the **T4** segment of the **F3T4** oligomer and the **BDP** chromophore. Importantly, the results also suggest that the efficiency of the partitioning varies with excitation wavelength, reinforcing the hypothesis that the structure of the Franck–Condon excited state in the **F3T4** diblock oligomer depends on the excitation wavelength.

Discussion

The investigation explored the photophysics of a series of fully π-conjugated "molecular wires" that feature distinct π-conjugated segments with distinct frontier orbital levels and HOMO–LUMO gaps. One aim of the work is to examine the dynamics of excited state (exciton) migration within the π-conjugated structures, and to explore how it depends on the structure and relative orientation of the π-conjugated segments. A second aim is to seek evidence for localization of the excited state that is initially formed by photoexcitation (*i.e.*, the Franck–Condon state) in the **F3T4** diblock oligomer. The results from a series of ultrafast spectroscopy provide clear insight regarding each of these aims, as well as other interesting and unexpected findings as outlined below.

The bichromophores **T4BDP** and **F3BDP** clearly demonstrate rapid excitation energy transfer from the π-conjugated oligomer segment to the **BDP** chromophore (*e.g.*, eqn (2a) and (3)). For **T4BDP**, well-resolved dynamics (Fig. 4b) indicate a transfer rate of $\sim 3 \times 10^{12}$ s^{-1}. Additionally, there is some evidence for photoinduced charge transfer from **T4** to BDP in **T4BDP** (eqn (2b)), supported by the emergence of a second near-IR band at 1000 nm shortly after excitation, likely corresponding to the cation radical $\mathbf{T4}^{+\bullet}$. Combined electrochemical and photophysical data indicate that the electron transfer process in (eqn (2b)) is exothermic by approximately 0.5 eV.

The fsTA study of diblock oligomer **F3T4** explored the early time spectra and dynamics to seek evidence for fast spectral changes that could be attributed to exciton relaxation on the **T4** segment. First, the absorption spectrum of **F3T4** has two bands located at 366 and 421 nm, which are associated with transitions mainly localized on the **F3** and **T4** segments. These assignments are supported by the TDDFT calculations (Tables S3 and S4) which identify transitions between orbitals mainly localized on **T4** at 445 nm ((406) HOMO → (407) LUMO) and on **F3** at 348 nm ((405) HOMO−1 → (408) LUMO+1). The fluorescence of **F3T4** shows a weak band that is close to the **F3** fluorescence, and a stronger band that is slightly red shifted, but shows similar vibronic structure to **T4**. This result shows that the relaxed exciton state that is responsible for the fluorescence is localized on **T4** but is stabilized by delocalization into the **F3** segment (Note that this effect is exciton delocalization, not charge transfer). Taken together, these results suggest that excitation of **F3T4** at a wavelength corresponding to the **F3** segment (~360 nm) could initially form an exciton that is mainly localized on **F3**. This exciton state would then undergo relaxation into the state where the exciton is mainly localized on the **T4** segment (Fig. 8).

The fsTA spectra of **F3T4** obtained with excitation at 363 nm corresponding to the **F3**-localized absorption transition are shown in Fig. 5. Here it is seen that within 13 ps the spectrum displays features that are definitively associated with the state where the exciton is localized on **T4**. Specifically, there are negative bands associated with the ground state bleach (GSB) of the **T4** absorption and stimulated emission (SE) of **T4** at 425 and 540 nm, and the prominent near-IR band due to **T4** excited state absorption (ESA) at 910 nm. Interestingly, the SE and ESA signals from the **T4** segment grow-in on a timescale of a few picoseconds, which is longer than the instrument rise-time. Fitting of the dominant rise component of the signal associated with the **T4** ESA at 919 nm suggests that the **F3** → **T4** exciton relaxation occurs with $\tau \sim 500$ fs ($k \sim 2 \times 10^{12}$ s^{-1}). Taken together, we conclude as shown in Fig. 8 that excitation at ~360 nm allows photoselection of an initial exciton state that is

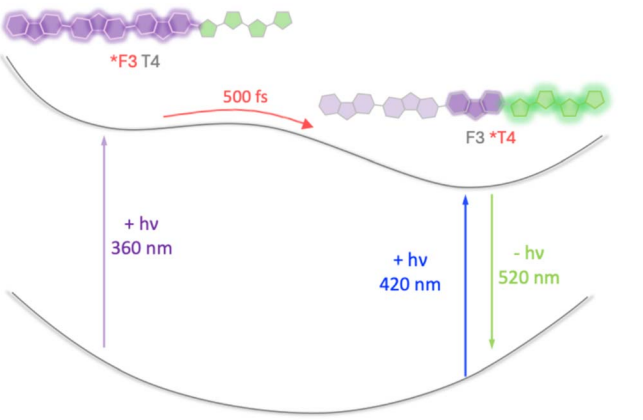

Fig. 8 Excited state scheme for F3T4. Highlights represent exciton localization.

mainly localized on the **F3** segment, and this state relaxes into the state where the exciton is localized on **T4** within 500 fs.

Now we turn to consider the trichromophores **F3T4BDP** and **T4F3BDP**. As noted previously, these oligomers are regio-isomers that differ in the "orientation" of the **BDP** chromophore relative to the diblock oligomer segment. Since the **BDP** excited state is lower in energy compared to the **F3** or **T4** localized exciton states, excitation transfer within **F3T4BDP** can be expected to be "vectorial" in nature, with an energy driven cascade of exciton transfer in the sequence **F3** → **T4** → **BDP** (Scheme 1). Thus, for this molecule, we do not expect significant effects of excitation wavelength (photoselection). By contrast for **T4F3BDP** vectorial exciton transfer is not possible, and we anticipated that the ultrafast exciton dynamics may be more complicated and exhibit photoselection.

As expected, the fsTA spectra and dynamics for **F3T4BDP** do not depend on excitation wavelength, and they indicate that rapidly following excitation the exciton is localized on the **BDP** chromophore. Thus, as shown in Fig. 9a, excitation of the **F3T4** diblock oligomer at 360 or 420 nm leads to ultrafast localization of the excitation on the **T4** segment, followed by transfer to the **BDP** chromophore. The last step is clearly resolved in the dynamics at 905 nm where the decay of the **T4** localized exciton occurs with $\tau \sim 1.7$ ps ($k \sim 6 \times 10^{11}$ s^{-1}).

Although the overall rapid vectorial movement of the exciton in **F3T4BDP** was expected, the experimental results revealed a complication that was unexpected. Inspection of the dynamics of the **T4** localized exciton at 905 nm (Fig. 6c and f) reveals that in addition to the fast decay, there is a longer-lived component with a lifetime that corresponds to that of the final **BDP**

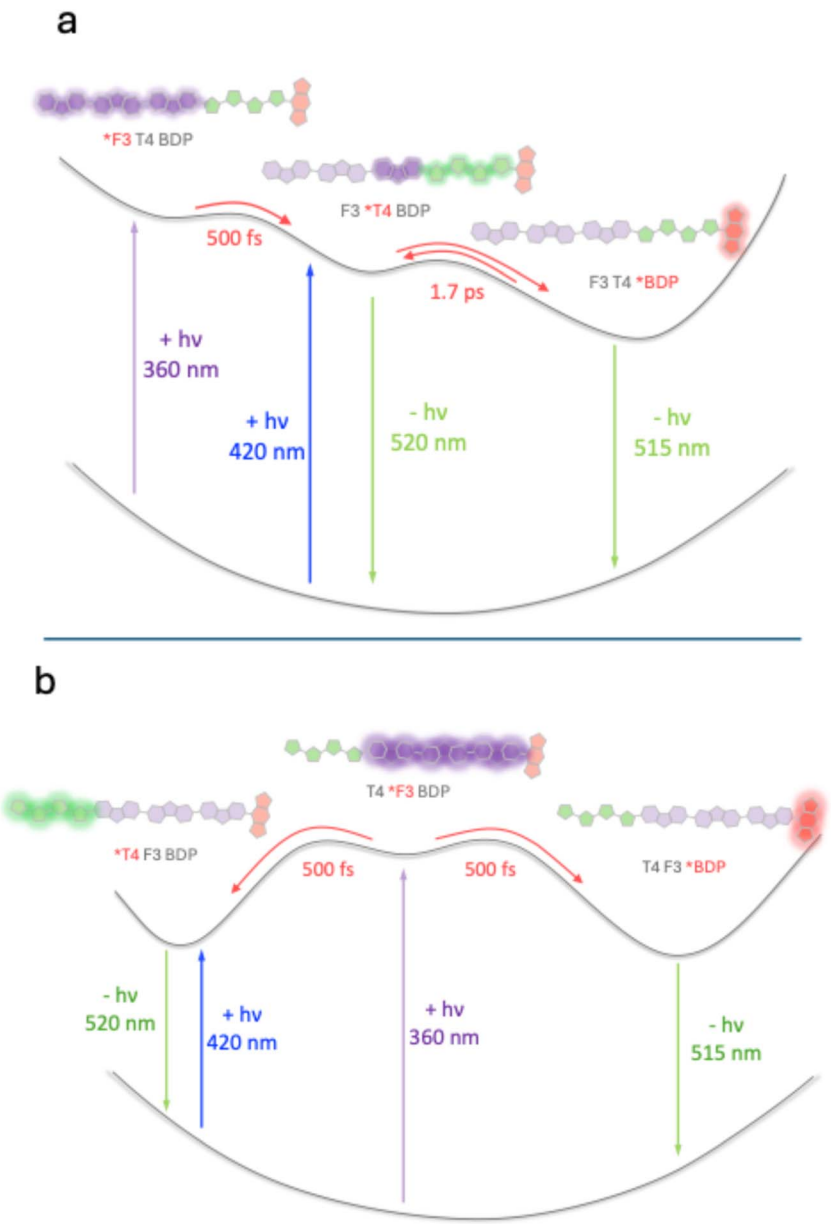

Fig. 9 Excited state schemes. Highlights represent exciton localization. (a) F3T4BDP. (b) T4F3BDP.

localized state (τ ~1.5 ns). We interpret this observation to indicate that following the initial ultrafast transfer of the exciton to **BDP**, an equilibrium is established between the **BDP** and **F3T4** localized exciton states. This occurs because the two excited states are very close in energy (compare the fluorescence of **T4BDP** and **F3T4** in Fig. 2a–c).

Unsurprisingly, the spectral evolution and dynamics of **T4F3BDP** are the most complex. First, excitation of **T4F3BDP** at 360 nm corresponding to the **F3** segment turns on a "bifurcation" in the exciton transport – some fraction relaxes towards the **T4** segment, while another fraction transfers to the **BDP** chromophore (Fig. 9b) (It is not possible to estimate the energy partitioning fraction, since we do not know the $\Delta\varepsilon$ values for the **BDP** GSB and **T4** ESA). Each of these states can be identified in Fig. 7a by their spectral signatures, *i.e.*, the **BDP** GSB at 507 nm and the **T4** ESA at 905 nm. Interestingly, these two states are not in equilibrium as confirmed by their different decay lifetimes (**T4** @905 nm, $\tau = 245$ ps and **BDP** @507 nm, $\tau = 2.8$ ns). This is likely due to the **F3** segment that serves as a spacer to isolate the **T4** and **BDP** chromophores.

Clear evidence for photoselection in the **F3T4** diblock oligomer comes by comparison of the **T4F3BDP** fsTA spectra with excitation at 420 nm corresponding to the **T4** segment with that at 350 nm corresponding to **F3** (Fig. 7a and d). There are significant differences in the spectra and dynamics when **T4F3BDP** is excited at 420 nm that strongly suggest that under these conditions the exciton partitioning favors **T4** over **BDP**. This is most evident by comparing the negative band between 500 and 600 nm for the two excitation wavelengths (Fig. 7a and d). Notably, the negative signal is distinctly broader under 420 nm excitation (Fig. 7d), which reflects a greater contribution of the **T4** SE to the signal than the **BDP** GSB which is narrower in bandwidth. The contribution of the **T4** SE to the total negative signal is also underscored by the fact that the kinetic fit at 507 nm shows a substantial lifetime component with $\tau = 251$ ps.

In summary, in the **F3T4BDP** polychromophore in which the segments are arranged to promote vectorial exciton transport, the results show that the system behaves as a molecular wire, with vectorial, highly efficient energy transfer taking place in less than 2 ps over a distance of 5 nm. By contrast, in **T4F3BDP** a "fork in the road" is introduced into the energy landscape that drives a bifurcation of the excitation energy between the two ends of the chromophore. This leads to formation of two distinct excited states that are not in equilibrium, displaying distinct decay rates characteristic of the localized exciton states.

A key question concerns the mechanism of exciton transport in the various molecular wires that are the focus of this study. Possible mechanisms include transport involving direct electronic coupling between the donor and (**BDP**) acceptor sites (*i.e.*, Dexter exchange coupling),[57] or direct "through-space" Förster transfer mediated by dipole–dipole coupling (FRET).[58] In order to probe the possibility for the FRET mechanism, we conducted calculations using the Förster equation for the four key structures, **F3BDP**, **T4BDP**, **F3T4BDP** and **T4F3BDP**. The calculations and a summary of transfer rates are provided in the supporting information section. In particular, Table S2 lists the calculated Förster overlap integrals (J), along with the calculated FRET transfer rates for a range of dipole–dipole orientations. For **T4BDP** and **F3T4BDP**, the calculated FRET rates are $>10^{12}$ s^{-1}, which is generally consistent with the observed rates (*e.g.* Fig. 4 and 6). By contrast, for **F3BDP**, the FRET calculation reveals a range of 5–30 $\times$ 10^{10} s^{-1}; this is noticably slower than is experimentally observed where the rate is clearly $>10^{12}$ s^{-1} (Fig. S57 and 58). Finally, most interesting is the calculation for **T4F3BDP**, which gives a rate for FRET in the range 1–8 $\times$ 10^{9} s^{-1}, which corresponds to a transfer lifetime of 130–760 ps. Quite interestingly, this calculation is in good agreement with the experimentally observed rate for the 250 ps decay component in **T4F3BDP** (Fig. 7). Taken together, the results indicate that for **T4BDP** and **F3T4BDP** the mechanism underlying the observed ultrafast transport cannot be unambiguously determined; it may involve FRET, direct coupling, or a combination of both. However, in **F3BDP** the observed rate is faster than predicted for FRET, suggesting that direct electronic coupling may dominate. Interestingly in **T4F3BDP**, the observed transfer rate is consistent with a mechanism involving through space FRET transfer from the **T4** localized exciton donor to the **BDP** acceptor.

Conclusions

This study explored the photophysics of a series of fully π-conjugated molecules consisting of a diblock oligomer with **F3** and **T4** segments that are linked on either end with a boron dipyrromethene (**BDP**) chromophore. The aim of the study was to explore the structure and dynamics of the excitons produced by excitation, with an emphasis on providing evidence for the ability to use excitation wavelength (photoselection) to influence the outcome of the exciton as it relaxes. The results find that regiochemistry of the oligomer structure influences the excited state dynamics. When the units are arranged to allow a vectorial energy landscape, the molecules act as "molecular wires", giving rise to rapid and relatively efficient energy transport to the **BDP** chromophore. By contrast, when the structure is inverted, vectorial transport is interrupted, and the molecules display a partitioning of the energy between the **BDP** chromophore and the **T4** segment of the diblock oligomer. In addition, the results provide clear evidence for photoselection in the partitioning, and this is evidence that the Franck Condon excited state in the **F3T4** oligomer features some degree of localization, either on the **F3** segment for near-UV excitation, or on the **T4** segment with blue-violet excitation. While previous studies have explored photophysical and photochemical outcomes of fully π-conjugated polychromophores,[6,12,26,27,29] this study is among the first to directly probe the exciton dynamics and structure in these systems on an ultrafast timescale.

Author contributions

Naresh Duvva: conceptualization, formal analysis, investigation, methodology, resources, validation, visualization, data curation, software, writing – original draft, writing – review and editing. Habtom B. Gobeze: formal analysis, data curation, investigation, resources, visualization, software, writing –

original draft, writing – review & editing. Isaí Barboza-Ramos: data curation, visualization, resources, software. Kirk S. Schanze: conceptualization, funding acquisition, investigation, project administration, supervision, methodology, data curation, resources, software, validation, visualization, writing – original draft, writing – review and editing.

Conflicts of interest

There are no conflicts to declare.

Data availability

The data supporting this article have been included as part of the SI. Supplementary Information: All experimental procedures, photophysical characterization, ultrafast transient absorption data, and synthetic procedures including characterizations. See DOI: **https://doi.org/10.1039/d5sc03704b**.

Acknowledgements

This work was supported by the Air Force Office of Scientific Research under Grant No. FA9550-23-1-0567 (AFOSR Materials Chemistry Program). Partial support was provided by the Welch Foundation through the Welch Chair at the University of Texas at San Antonio (Award No. AX-0045-20110629). We thank Dr Tanjila Islam for help with conducting the DFT and TDDFT calculations. We also acknowledge the Texas Advanced Computing Center (TACC) at the University of Texas at Austin for providing high-performance computing (HPC) resources that have contributed to the research results reported in this article.

References

1 R. P. Feynman, *There's Plenty of Room at the Bottom*, **https://www.zyvex.com/nanotech/feynman.html**.
2 A. Aviram and M. A. Ratner, *Chem. Phys. Lett.*, 1974, **29**, 277–283.
3 R. W. Wagner and J. S. Lindsey, *J. Am. Chem. Soc.*, 1994, **116**, 9759–9760.
4 D. K. James and J. M. Tour, in *Molecular Wires and Electronics*, Springer Berlin Heidelberg, Berlin, Heidelberg, 2005, pp. 33–62, DOI: **10.1007/b136066**.
5 Y. Shibano, H. Imahori, P. Sreearunothai, A. R. Cook and J. R. Miller, *J. Phys. Chem. Lett.*, 2010, **1**, 1492–1496.
6 M. Gilbert and B. Albinsson, *Chem. Soc. Rev.*, 2015, **44**, 845–862.
7 M. J. Bird, O. G. Reid, A. R. Cook, S. Asaoka, Y. Shibano, H. Imahori, G. Rumbles and J. R. Miller, *J. Phys. Chem. C*, 2014, **118**, 6100–6109.
8 L. Zaikowski, G. Mauro, M. Bird, B. Karten, S. Asaoka, Q. Wu, A. R. Cook and J. R. Miller, *J. Phys. Chem. B*, 2015, **119**, 7231–7241.
9 W. B. Davis, W. A. Svec, M. A. Ratner and M. R. Wasielewski, *Nature*, 1998, **396**, 60–63.
10 W. B. Davis, M. A. Ratner and M. R. Wasielewski, *J. Am. Chem. Soc.*, 2001, **123**, 7877–7886.
11 E. A. Weiss, M. J. Ahrens, L. E. Sinks, A. V. Gusev, M. A. Ratner and M. R. Wasielewski, *J. Am. Chem. Soc.*, 2004, **126**, 5577–5584.
12 R. H. Goldsmith, L. E. Sinks, R. F. Kelley, L. J. Betzen, W. Liu, E. A. Weiss, M. A. Ratner and M. R. Wasielewski, *Proc. Natl. Acad. Sci. U. S. A.*, 2005, **102**, 3540–3545.
13 J. Wiberg, L. Guo, K. Pettersson, D. Nilsson, T. Ljungdahl, J. Mårtensson and B. Albinsson, *J. Am. Chem. Soc.*, 2007, **129**, 155–163.
14 B. Albinsson, M. P. Eng, K. Pettersson and M. U. Winters, *Phys. Chem. Chem. Phys.*, 2007, **9**, 5847–5864.
15 C. Schubert, J. T. Margraf, T. Clark and D. M. Guldi, *Chem. Soc. Rev.*, 2015, **44**, 988–998.
16 M.-K. Ng, D.-C. Lee and L. Yu, *J. Am. Chem. Soc.*, 2002, **124**, 11862–11863.
17 M.-K. Ng and L. Yu, *Angew Chem. Int. Ed. Engl.*, 2002, **41**, 3598–3601.
18 T. Dadosh, Y. Gordin, R. Krahne, I. Khivrich, D. Mahalu, V. Frydman, J. Sperling, A. Yacoby and I. Bar-Joseph, *Nature*, 2005, **436**, 677–680.
19 R. Huber, M. T. González, S. Wu, M. Langer, S. Grunder, V. Horhoiu, M. Mayor, M. R. Bryce, C. Wang, R. Jitchati, C. Schönenberger and M. Calame, *J. Am. Chem. Soc.*, 2008, **130**, 1080–1084.
20 L. Lafferentz, F. Ample, H. Yu, S. Hecht, C. Joachim and L. Grill, *Science*, 2009, **323**, 1193–1197.
21 V. Kaliginedi, P. Moreno-García, H. Valkenier, W. Hong, V. M. García-Suárez, P. Buiter, J. L. H. Otten, J. C. Hummelen, C. J. Lambert and T. Wandlowski, *J. Am. Chem. Soc.*, 2012, **134**, 5262–5275.
22 P. Moreno-García, M. Gulcur, D. Z. Manrique, T. Pope, W. Hong, V. Kaliginedi, C. Huang, A. S. Batsanov, M. R. Bryce, C. Lambert and T. Wandlowski, *J. Am. Chem. Soc.*, 2013, **135**, 12228–12240.
23 R. M. Metzger, *Chem. Rev.*, 2015, **115**, 5056–5115.
24 W.-Y. Lo, N. Zhang, Z. Cai, L. Li and L. Yu, *Acc. Chem. Res.*, 2016, **49**, 1852–1863.
25 C. Sagan, Y. Jiang, F. Caban, J. Snaider, R. Amell, S. Wei and G. M. Florio, *J. Phys. Chem. C*, 2017, **121**, 24945–24953.
26 C. Devadoss, P. Bharathi and J. S. Moore, *J. Am. Chem. Soc.*, 1996, **118**, 9635–9644.
27 V. S. Y. Lin, S. G. DiMagno and M. J. Therien, *Science*, 1994, **264**, 1105–1111.
28 D. Beljonne, G. Pourtois, C. Silva, E. Hennebicq, L. M. Herz, R. H. Friend, G. D. Scholes, S. Setayesh, K. Müllen and J. L. Brédas, *Proc. Natl. Acad. Sci. U.S.A.*, 2002, **99**, 10982–10987.
29 J. M. Keller, K. D. Glusac, E. O. Danilov, S. McIlroy, P. Sreearuothai, A. R. Cook, H. Jiang, J. R. Miller and K. S. Schanze, *J. Am. Chem. Soc.*, 2011, **133**, 11289–11298.
30 R. J. Dillon, Z. Pan, J. Jiang, R. W. Winkel, J. M. Papanikolas and K. S. Schanze, *J. Phys. Chem. C*, 2020, **124**, 18920–18929.
31 O. P. Dimitriev, *Chem. Rev.*, 2022, **122**, 8487–8593.
32 A. C. Grimsdale, K. Leok Chan, R. E. Martin, P. G. Jokisz and A. B. Holmes, *Chem. Rev.*, 2009, **109**, 897–1091.

33 L. Lu, T. Zheng, Q. Wu, A. M. Schneider, D. Zhao and L. Yu, *Chem. Rev.*, 2015, **115**, 12666–12731.
34 L. Dou, Y. Liu, Z. Hong, G. Li and Y. Yang, *Chem. Rev.*, 2015, **115**, 12633–12665.
35 P. Gu, Y. Yao, L. Feng, S. Niu and H. Dong, *Polym. Chem.*, 2015, **6**, 7933–7944.
36 D. T. McQuade, A. E. Pullen and T. M. Swager, *Chem. Rev.*, 2000, **100**, 2537–2574.
37 L. Stryer and R. P. Haugland, *Proc. Natl. Acad. Sci. U.S.A.*, 1967, **58**, 719–726.
38 H. E. Zimmerman and R. D. McKelvey, *J. Am. Chem. Soc.*, 1971, **93**, 3638–3645.
39 H. E. Zimmerman, T. D. Goldman, T. K. Hirzel and S. P. Schmidt, *J. Org. Chem.*, 1980, **45**, 3933–3951.
40 G. L. Closs and J. R. Miller, *Science*, 1988, **240**, 440–447.
41 G. L. Closs, M. D. Johnson, J. R. Miller and P. Piotrowiak, *J. Am. Chem. Soc.*, 1989, **111**, 3751–3753.
42 P. F. H. Schwab, M. D. Levin and J. Michl, *Chem. Rev.*, 1999, **99**, 1863–1934.
43 P. F. H. Schwab, J. R. Smith and J. Michl, *Chem. Rev.*, 2005, **105**, 1197–1280.
44 S. S. Isied, M. Y. Ogawa and J. F. Wishart, *Chem. Rev.*, 1992, **92**, 381–394.
45 M. R. Wasielewski, *Chem. Rev.*, 1992, **92**, 435–461.
46 D. Gust, T. A. Moore and A. L. Moore, *Acc. Chem. Res.*, 1993, **26**, 198–205.
47 B. Shan, A. Nayak, O. F. Williams, D. C. Yost, N. F. Polizzi, Y. Liu, N. Zhou, Y. Kanai, A. M. Moran, M. J. Therien and T. J. Meyer, *Proc. Natl. Acad. Sci. U.S.A.*, 2019, **116**, 16198–16203.
48 J. Jiang, A. Alsam, S. Wang, S. M. Aly, Z. Pan, O. F. Mohammed and K. S. Schanze, *J. Phys. Chem. A*, 2017, **121**, 4891–4901.
49 A. L. Jones, M. K. Gish, C. J. Zeman, J. M. Papanikolas and K. S. Schanze, *J. Phys. Chem. A*, 2017, **121**, 9579–9588.
50 M. K. Gish, A. L. Jones, J. M. Papanikolas and K. S. Schanze, *J. Phys. Chem. C*, 2018, **122**, 18802–18808.
51 H. B. Gobeze, M. Younus, M. D. Turlington, S. Ahmed and K. S. Schanze, *Molecules*, 2024, **29**, 2678.
52 H. B. Gobeze, D. Martinez and K. S. Schanze, *J. Photochem. Photobiol., A*, 2023, **444**, 114966.
53 H. B. Gobeze, P. Jagadesan and K. S. Schanze, *Phys. Chem. Chem. Phys.*, 2023, **25**, 23685–23695.
54 A. L. Jones, J. Jiang and K. S. Schanze, *J. Am. Chem. Soc.*, 2020, **142**, 12658–12668.
55 Y. Zhao, S. R. Valandro, M. Younus, H. B. Gobeze and K. S. Schanze, *CCS Chem.*, 2025, **7**, 2293–2303.
56 G. J. Hedley, A. Ruseckas, A. C. Benniston, A. Harriman and I. D. W. Samuel, *J. Phys. Chem. A*, 2015, **119**, 12665–12671.
57 D. L. Dexter, T. Forster and R. S. Knox, *Phys. Status Solidi*, 1969, **34**, K159.
58 T. Förster, *Ann. Phys.*, 1948, **437**, 55–75.